Experimental and Theoretical Characterization of Electrode Materials that Undergo Large Volume Changes and Application to the Lithium–Silicon System

ARTICLE *in* THE JOURNAL OF PHYSICAL CHEMISTRY C · MARCH 2015

Impact Factor: 4.77 · DOI: 10.1021/jp512585z

5 AUTHORS, INCLUDING:

Xingcheng Xiao
General Motors Company
175 PUBLICATIONS **2,636** CITATIONS
SEE PROFILE

Qinglin Zhang
University of Kentucky
14 PUBLICATIONS **51** CITATIONS
SEE PROFILE

Yang-Tse Cheng
University of Kentucky
180 PUBLICATIONS **5,942** CITATIONS
SEE PROFILE

THE JOURNAL OF PHYSICAL CHEMISTRY C

Article

pubs.acs.org/JPCC

Experimental and Theoretical Characterization of Electrode Materials that Undergo Large Volume Changes and Application to the Lithium−Silicon System

Mark W. Verbrugge,*[,†] Daniel R. Baker,[†] Xingcheng Xiao,[†] Qinglin Zhang,[‡] and Yang-Tse Cheng[‡]

[†]General Motors Research and Development Chemical and Materials Systems Laboratory 30500 Mound Road, Warren, Michigan 48090-0955, United States

[‡]University of Kentucky Department of Chemical and Materials Engineering 177 FPAT, Lexington, Kentucky 40506-0046, United States

Supporting Information

ABSTRACT: The life and performance of lithium-ion batteries are related to the mechanical expansion and contraction of the active materials, particularly for silicon-enhanced negative electrodes. In this work, we develop a theory and commensurate equations to describe how lithium diffuses within lithiated silicon, and we include the influence of active material expansion (upon lithiation) and contraction (upon delithiation). The treatment of diffusion is based on irreversible thermodynamics, and a charge-transfer relationship is employed at the electrode−electrolyte interface. The experimental approach allows us to isolate our analysis to the active material and avoids the necessity of treating binders, conductive diluents, and complicated geometries associated with conventional porous electrodes used in most practical lithium-ion batteries and in the construction and modeling of a Li−Si porous electrode. The model is shown to compare favorably with experimental results. The final section of this paper addresses significant open questions.

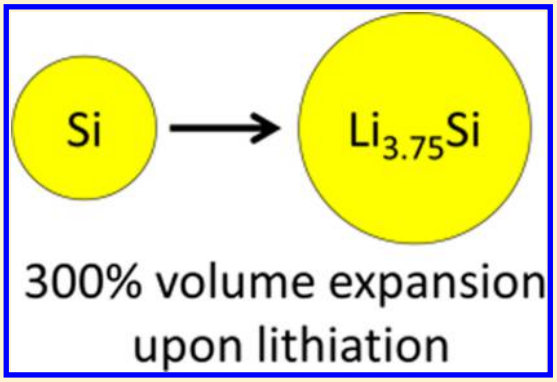

INTRODUCTION

Lithium (Li) is the lightest element that is a solid at room temperature. Its compounds and alloys, when combined with nonaqueous aprotic electrolytes,[1,2] yield battery systems with the highest energy and power density available today for most applications, including automotive traction systems. As we transition from today's Li-ion battery systems[3−9] to those of the next generation,[10] in particular, for extended-range electric vehicles (EREVs, such as the Chevrolet Volt) and for battery-electric vehicles (BEVs, such as the Chevrolet Spark EV), the electrode materials are expected to accommodate higher Li concentrations. However, empirical evidence shows clearly that such increased Li content will yield greater expansion of the active materials upon lithiation,[11,12] and a corresponding volume contraction on delithiation, consistent with Vegard's Law governing qualitatively the characteristics of materials, including Li−Si systems.[13] It is therefore important to understand how such volume changes are linked to, and impact, electrochemical phenomena, and that is the purpose of this research.

We employ thin films of vapor-deposited Si to construct our electrodes. This allows us to restrict our analysis to the active material and avoids the necessity of treating binders, conductive diluents, and complicated geometries associated with conventional porous electrodes[14−17] used in most practical lithium-ion batteries. It also avoids the complexity of the construction and modeling of a Li−Si porous electrode.[18] The utility of thin Si films for the characterization of the Li−Si system is well established.[19−31]

The next section outlines the theoretical underpinnings of our approach, after which we describe the experimental methods and procedures, discuss the results of this work, and, last, overview open questions associated with this line of research and development.

THEORY AND MODEL DEVELOPMENT

Thermodynamics and Electrochemistry. A schematic of the cell configuration is shown in Figure 1. We consider the electrochemical reaction of lithium with a thin-film active material (Si) of the type

$$Li^+ + e^- + Host \underset{k_a}{\overset{k_c}{\rightleftarrows}} Li{-}Host \quad (1)$$

where Li^+ is a lithium ion in the electrolyte, Host represents a vacant site without lithium in the host material, and Li−Host represents a site occupied by a lithium atom, and this corresponds

Received: December 17, 2014
Revised: February 1, 2015
Published: February 25, 2015

DOI: 10.1021/jp512585z
J. Phys. Chem. C 2015, 119, 5341−5349

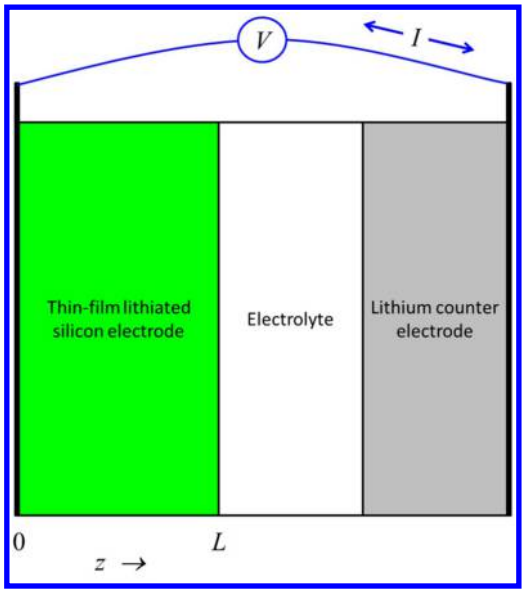

Figure 1. Cell schematic. For this work, the Li−Si electrode was 67 nm thick.

to the Li species within the active material. We shall represent Host by a subscript "H", in what follows. We shall extend the existing site model[16,17,32−34] to accommodate volume changes. Our nomenclature (cf. Table 1) will be such that quantities pertaining to lithium-filled sites are not subscripted.[34] At constant temperature and pressure, the open-circuit potential U of the active material with respect to a metallic lithium electrode is given as

$$-FU(x) = \mu(x) - \mu_{\mathrm{H}}(x) - \mu_{\mathrm{Li}}^{\mathrm{ref}} \tag{2}$$

where μ is the chemical potential of the lithium within the working electrode, x is the mole fraction of sites available for lithium that are occupied by lithium within the active material, and $\mu_{\mathrm{Li}}^{\mathrm{ref}}$ is the chemical potential of the metallic lithium reference electrode (Note: $x + x_{\mathrm{H}} = 1$). We shall ignore the influence of stress on the thermodynamics and transport of the Li−Si thin films.[35−38,41] As has been shown, when one neglects the influence of temperature and stress,[16,17,32−34] it is possible to extract the lithium activity coefficient directly from a plot of $U(x)$ versus x:

$$\frac{F}{RT}(1-x)\frac{\mathrm{d}U}{\mathrm{d}\ln x} = -\left(1 + \frac{\mathrm{d}\ln\gamma}{\mathrm{d}\ln x}\right) = \frac{F}{RT}(1-x)x\frac{\mathrm{d}U}{\mathrm{d}x} \tag{3}$$

Shown in Figure 2 are U and $\mathrm{d}x/\mathrm{d}U$ versus x; for the purposes of this work, we employ a look-up table populated by the data to evaluate $U(x)$ and $\mathrm{d}U/\mathrm{d}x$. We treat charge (lithium ion reduction at the electrode surface) and discharge (lithium oxidation at the electrode surface) events separately, each having their own look-up table, and we do not treat further the hysteresis in $U(x)$. Despite the large fractional volume change of the Li−Si system during operation, work associated with volume expansion is negligible for the thin-film electrode operating at atmospheric pressure, and it is neglected in our thermodynamic treatment. The full description of the equilibrium potential, including the influence of temperature, stress, and potential hysteresis, remains an important open problem (see the open questions at the end of this document).

At the electrode−solution interface (cf. Figure 1), we treat the charge-transfer (electrochemical) reaction as a single-electron

Table 1. Nomenclature[a]

a_i	see eq 9, mol/cm^3
A	geometric (plan view) area of the electrode, cm^2
c	salt concentration in electrolyte, mol/cm^3
c_{ref}	reference salt concentration in electrolyte, mol/cm^3
c_{T}	total concentration of sites (eq 7), mol/cm^3
D	diffusion coefficient of lithium filled sites (Li−Host species), cm^2/s
F	Faraday constant, 96487 C/mol
i	current density, A/cm^2
i_0^{ref}	reference exchange current density, a constant, A/cm^2
L	thin-film electrode thickness, cm
MW	molecular weight, g/mol
N	flux of lithium-filled sites, mol/cm^2·s
N_{H}	flux of vacant (Host) sites, mol/cm^2·s
N_{T}	total flux of sites, $N + N_{\mathrm{H}}$, mol/cm^2·s
Q	charge, C
R	gas constant, 8.314 J/mol·K
t	time, s
T	temperature, K
U	open-circuit voltage, V
V	electrode voltage with respect to a lithium reference, V
$Vl_{x=0}$	electrode volume at $x = 0$ (eq 8), cm^3
Vl_x	electrode volume at mole fraction x (eq 8), cm^3
w	dimensionless transformed position coordinate, $w = z/L(t)$ and $0 \le w \le 1$
x	mole fraction of lithium filled sites (Li−Host species)
z	position coordinate, cm
α	dimensionless parameter reflecting the importance of diffusion resistance to that of charge transfer (eq 22)
β	symmetry factor
γ	activity coefficient of Li-filled sites
η_{s}	surface overpotential, V
μ	chemical potential of Li-filled sites, J/mol
μ_{H}	chemical potential of vacant sites, J/mol
ν	sweep rate for voltage source, V/s
τ	dimensionless time (eq 22)
ξ	maximum number of lithium atoms per Si host ($\xi = 4.4$, see text below eq 6)

[a]A tilde over a variable represents a dimensionless form of the variable (eqs 22 and 23).

elementary reaction, and we neglect the influence of any surface layers such as that of a solid-electrolyte interphase. This approach has worked well in modeling of lithiated graphite (single-fiber) electrodes:[32]

$$i = i_0^{\mathrm{ref}} x^{\beta}\left[\frac{c}{c_{\mathrm{ref}}}(1-x)\right]^{1-\beta}\left[e^{(1-\beta)F\eta_{\mathrm{s}}/RT} - e^{-\beta F\eta_{\mathrm{s}}/RT}\right]$$

$$\text{and } \eta_{\mathrm{s}} = V - U \tag{4}$$

Anodic (discharge) currents correspond to positive surface overpotential η_{s} and current i. The symmetry factor β and the reference exchange current density i_0^{ref} are constants. The form of eq 4 is common to modeling investigations of lithium ion batteries.[14−17,32−34] The electrolyte salt concentration is given by c; in the absence of concentration variations in the electrolyte, $c/c_{\mathrm{ref}} = 1$; we find this approximation appropriate, as Li diffusion within Li−Si is quite slow relative to diffusion within the liquid phase.

Solid-State Diffusion. We model the transport of lithium-filled sites ("Li−Host" in eq 1) within the active material using irreversible thermodynamics. Section 18.4 of ref 39 provides historical context; the specific equations we employ can be

DOI: 10.1021/jp512585z
J. Phys. Chem. C 2015, 119, 5341−5349

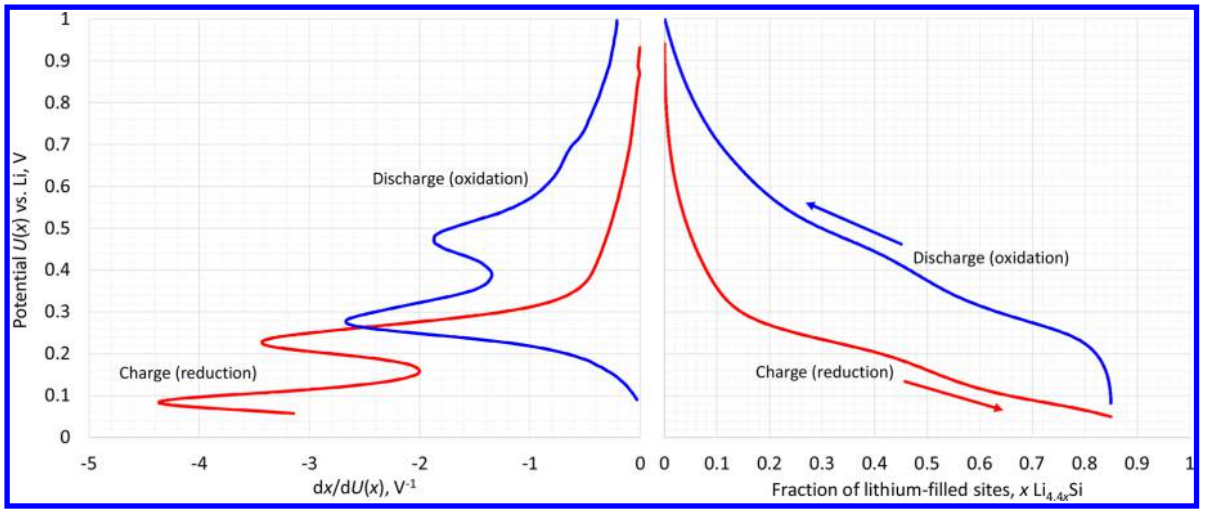

Figure 2. Left: Differential voltage spectroscopy plot. Right: Open-circuit potential as a function of Li content. The ordinate label is common to both plots.

derived easily from section 12.1 of ref 15 and appear in refs 16, 17, and 32−34. The net flux of lithium N is given by

$$\begin{aligned} N &= -c_T x \frac{D}{RT}\nabla\mu + x(N + N_H) \\ &= -c_T D\left(1 + \frac{d\ln\gamma}{d\ln x}\right)\nabla x + x(N + N_H) \\ &= c_T D\frac{F}{RT}x(1-x)\frac{\partial U}{\partial x}\nabla x + x(N + N_H) \end{aligned} \quad (5)$$

where N_H is the flux of the unoccupied Li sites within the electrode ("Host" in eq 1), c_T is the concentration of sites available for Li, and D is the diffusion coefficient. Thus, the net flux of lithium-filled sites (left side) corresponds to diffusive flux driven by gradients in the chemical potential $\nabla\mu$ and augmented by the lithium fraction of the total flux of $x(N + N_H)$. The total concentration of sites available for lithium c_T of the Li−Si material is taken to be a function of lithium content:

$$c_T = c_T(x) \quad (6)$$

Thus, at any given time, some of the sites will be vacant and some will be filled with lithium; the sum of the filled and vacant sites is given by c_T. Relative to the formula $Li_{\xi x}Si$, it is often reported that $\xi = 4.4$, although this level of lithiation is not seen in electrochemical experiments.[40] The change in mass density with x in $Li_{\xi x}Si$ is known for crystalline Li−Si,[42] and we use such data in this work, although we expect the Li−Si to become substantially amorphous upon cycling. From such data, we can determine c_T:

$$c_T(x) = \frac{\rho_{Li_{\xi x}Si}}{MW_{Li_{\xi x}Si}}\xi \quad (7)$$

where ρ represents mass density and MW denotes molecular weight. Because (1) we assume the geometric area A (plan view) of the electrode does not change and (2) the total moles of sites, be they filled or unfilled, does not change, the thickness of the thin-film electrode that is devoid of Li relative to the lithiated state is given by

$$\frac{V|_{x=0}}{V|_x} = \frac{AL|_{x=0}}{AL|_x} = \frac{c_T|_x}{c_T|_{x=0}} \text{ or } \frac{L(x)}{L_0} = \frac{\xi c_{Si,x=0}}{c_T(x)} = \frac{c_{T,0}}{c_T(x)} \quad (8)$$

We ignore the influence of stress on the thermodynamics and transport of the Li−Si thin films. Instead, we use a one-dimensional model, which assumes that stress does not impact the chemical potential, because the stresses are negligible within the infinitely thin film that is viewed as mechanically unconstrained at the electrode−electrolyte interface. Thus, eq 6 represents a local equilibrium condition. Equation 7 was used to calculate $c_T(x)$ from available data,[42] which is displayed in Figure 3, with the solid line represented by

$$\begin{aligned} c_T(x) &= \sum_{j=0}^{2} a_j x^j \\ a_0 &= 0.365\ \text{mol/cm}^3 \\ a_1 &= -0.551\ \text{mol/cm}^3 \\ a_2 &= 0.279\ \text{mol/cm}^3 \end{aligned} \quad (9)$$

Equations 5 and 6 can be viewed as phenomenological; along with material balances to be described, the mathematical description for the system can be completed. A material balance on Li in combination with eq 6 yields

$$\frac{\partial c}{\partial t} = -\nabla\cdot N \text{ or } \left(x\frac{dc_T}{dx} + c_T\right)\frac{\partial x}{\partial t} = -\nabla\cdot N \quad (10)$$

A material balance on the total moles yields

$$\frac{\partial c_T}{\partial t} = -\nabla\cdot N_T = -\nabla\cdot(N + N_H)$$

which, when combined with eq 6, yields

$$\frac{dc_T}{dx}\frac{\partial x}{\partial t} = -\nabla\cdot(N + N_H) \quad (11)$$

For initial conditions, the particle is equilibrated with the initial electrode potential and the lithium mole fraction is constant throughout the film:

$$x(0, z) = x_{init} = x(U_{init}) \quad (12)$$

DOI: 10.1021/jp512585z
J. Phys. Chem. C 2015, 119, 5341−5349

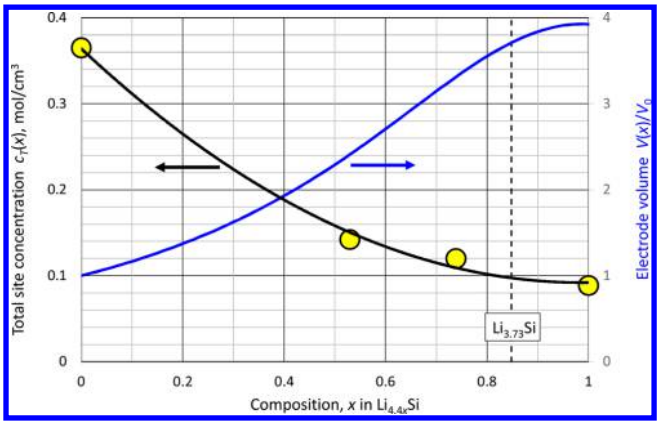

Figure 3. Total concentration of sites based on literature values[42] for the unit-cell volumes (left) and corresponding site concentration $c_T(x)$. In going from pure Si to $Li_{4.4}Si$, the volume per mole of Si increases by just under 300%. In this work, we examine equilibrium potentials ranging from 50 mV to 1 V, corresponding to $x = 0$ to $x = 0.848$, or pure Si to $Li_{3.73}Si$, respectively, and yielding a 271% expansion. The solid for $c_T(x)$ corresponds to eq 9; the fractional volume is given by $c_T(0)/c_T(x)$ (see eq 8).

Neither Li-filled sites nor vacant sites enter the current collector, facts that provide boundary conditions at the interface between the current collector and the active material:

$$N|_{z=0,t} = 0 \tag{13}$$

$$N_H|_{z=0,t} = 0 \tag{14}$$

The dependent variables in these equations are the mole fraction x and the fluxes N and N_H. The first-order field equations for the fluxes, eqs 10 and 11, require two additional boundary conditions for electrode−electrolyte interface position $z = L(t)$. Total molar balances on the lithium-filled sites and the vacant sites can be employed to generate the two conditions. A molar balance on sites filled with Li within the entire film leads to

$$\int_0^{L(t)} c(t, z)\mathrm{d}z = \int_0^{L(0)} c(0, z)\mathrm{d}z - \int_0^t \frac{i(\bar{t})}{F}\mathrm{d}\bar{t}, \quad c = xc_T \tag{15}$$

Similarly, we can write for the filled sites

$$\int_0^{L(t)} c_H(t, z)\mathrm{d}z = \int_0^{L(0)} c_H(t = 0, z)\mathrm{d}z + \int_0^t \frac{i(\bar{t})}{F}\mathrm{d}\bar{t}, \quad c_H = (1 - x)c_T \tag{16}$$

Upon differentiation with respect to time, these two independent equations can be recast in a form convenient for analysis (see Supporting Information):

$$\frac{\mathrm{d}L}{\mathrm{d}t} = \frac{N_T}{c_T} = \frac{1}{c_T}(N + N_H) \tag{17}$$

and

$$N - x(N + N_H) = \frac{i}{F} \tag{18}$$

Both sides of eq 17 have units of velocity (distance/time). Thus, the growth rate of the film corresponds to the total molar velocity evaluated at the surface of the film. For equimolar counter diffusion,[39,43] as has been employed for systems such as lithiated graphite that show little volume change during lithium insertion and extraction,[16,17,34] c_T is nearly constant for all values of x, $N_T = N + N_H = 0$, and $\mathrm{d}L/\mathrm{d}t = 0$. Similarly, for equimolar counter diffusion, $N = -N_H$, and eq 18 yields the commonly used expression at the electrode−electrolyte interface, $N = i/F$.

Equation 4 is specified at a moving boundary, since the electrode−electrolyte interface at $z = L(t)$ will move as the electrode expands and contracts. It is expeditious to formulate the equation system such that the position of the moving boundary can be determined simultaneously as part the solution to the entire equation system.[44] Define $w = z/L(t)$. Then

$$\frac{\partial}{\partial z} = \frac{\partial w}{\partial z}\frac{\partial}{\partial w} = \frac{1}{L(t)}\frac{\partial}{\partial w}$$

$$\frac{\partial}{\partial t} = \frac{\partial w}{\partial t}\frac{\partial}{\partial w} + \frac{\partial}{\partial t} = -\frac{w}{L(t)}\frac{\mathrm{d}L}{\mathrm{d}t}\frac{\partial}{\partial w} + \frac{\partial}{\partial t}$$

We can now transform the entire problem onto the region $0 \le w \le 1$ as follows. Equations 5, 10, and 11 become

$$N = c_T D\frac{F}{RT}x(1 - x)\frac{\partial U}{\partial x}\frac{1}{L(t)}\frac{\partial x}{\partial w} + x(N + N_H) \tag{19}$$

$$\left(x\frac{\mathrm{d}c_T}{\mathrm{d}x} + c_T\right)\left(\frac{\partial x}{\partial t} - \frac{w}{L(t)}\frac{\mathrm{d}L}{\mathrm{d}t}\frac{\partial x}{\partial w}\right) = -\frac{1}{L(t)}\frac{\partial N}{\partial w} \tag{20}$$

$$\frac{\mathrm{d}c_T}{\mathrm{d}x}\left(\frac{\partial x}{\partial t} - \frac{w}{L(t)}\frac{\mathrm{d}L}{\mathrm{d}t}\frac{\partial x}{\partial w}\right) = -\frac{1}{L(t)}\frac{\partial(N + N_H)}{\partial w} \tag{21}$$

Equations 6, 12, 13, 14, 17, and 18 still hold as written. Table 2 provides a recapitulation of the dimensioned equation system.

To scale the problem and identify governing dimensionless groups, the following definitions are employed.

$$\tilde{c}_T = \frac{c_T}{c_{T,0}} \quad \tilde{D} = \frac{D}{D_0} \quad \tilde{i} = \frac{L_0}{D_0 c_{T,0}}\frac{i}{F}$$

$$\tilde{L} = \frac{L}{L_0} \quad \tilde{N} = \frac{L_0}{D_0 c_{T,0}}N \quad \tilde{U} = \frac{F}{RT}U$$

$$\tilde{V} = \frac{F}{RT}V \quad \alpha = \frac{L_0}{D_0 c_{T,0}}\frac{i_0^{ref}}{F} \quad \tau = \frac{D_0}{L_0^2}t \tag{22}$$

With the exception of the exchange current density i_0^{ref}, a subscript of 0 in eq 22 denotes evaluation at $x = 0$ (infinitely dilute Li). The dimensionless form of the equation system is provided in Table 3. With reference to eqs 9 and 22,

$$\tilde{c}_T(x) = \sum_{j=0}^{2} \tilde{a}_j x^j \text{ and } \frac{\mathrm{d}\tilde{c}_T}{\mathrm{d}x} = \sum_{j=1}^{2} j\tilde{a}_j x^{j-1}$$

$$\tilde{a}_0 = 1$$

$$\tilde{a}_1 = -1.510$$

$$\tilde{a}_2 = 0.7644 \tag{23}$$

The nonlinear, coupled equation system described in Table 3 was solved by the referenced finite-difference routine.[45]

EXPERIMENTAL METHODS AND PROCEDURES

Silicon thin-film electrodes were deposited on copper current collectors in a radio frequency magnetron sputtering system (Angstrom Engineering Åmod System) that is integrated with an Ar-filled glovebox. The RF power is 240 W, and the Ar

DOI: 10.1021/jp512585z
J. Phys. Chem. C 2015, 119, 5341−5349

Table 2. Dimensioned Equation System[a]

current collector, $z = 0$, $w = 0$	electrode, $0 < z < L$, $0 < w < 1$	electrode−electrolyte interface, $z = L(t)$, $w = 1$
$N = 0$	$N = c_T D \frac{F}{RT} x(1-x) \frac{\partial U}{\partial x} \frac{1}{L(t)} \frac{\partial x}{\partial w} + x(N + N_H)$	$N = c_T D \frac{F}{RT} x(1-x) \frac{\partial U}{\partial x} \frac{1}{L(t)} \frac{\partial x}{\partial w} + x(N + N_H)$
$(\partial x/\partial w) = 0$	$\left(x \frac{dc_T}{dx} + c_T\right)\left(\frac{\partial x}{\partial t} - \frac{w}{L(t)} \frac{dL}{dt} \frac{\partial x}{\partial w}\right) = -\frac{1}{L(t)} \frac{\partial N}{\partial w}$	$(1-x)N - xN_H =$ $\begin{cases} \frac{i}{F} & \text{current control} \\ \frac{i_0^{ref}}{F} x^{\beta}(1-x)^{1-\beta}\left[e^{(1-\beta)F(V-U)/RT} - e^{-\beta F(V-U)/RT}\right] & \text{potential control} \end{cases}$
$N_H = 0$	$\frac{dc_T}{dx}\left(\frac{\partial x}{\partial t} - \frac{w}{L(t)} \frac{dL}{dt} \frac{\partial x}{\partial w}\right) = -\frac{1}{L(t)} \frac{\partial (N + N_H)}{\partial w}$	$\frac{dc_T}{dx}\left(\frac{\partial x}{\partial t} - \frac{w}{L(t)} \frac{dL}{dt} \frac{\partial x}{\partial w}\right) = -\frac{1}{L(t)} \frac{\partial (N + N_H)}{\partial w}$ $c_T \frac{dL}{dt} = N + N_H$

[a]The four rows of equations can be used to solve for the unknowns x, N, N_H, and L. The total molar concentration c_T is a known (measured) function of the composition (lithium site fraction x). Initially, the fluxes N and N_H are zero, the lithium concentration is uniform, $x(0,w) = x_{init}$, and the film has an initial thickness $L(0) = L(x_{init})$. The second line for the lithium flux expression at the electrode−electrolyte interface indicates that either the cell current density i or the potential V can be controlled.

Table 3. Dimensionless Equation System[a]

current collector, $w = 0$	electrode, $0 < w < 1$	electrode−electrolyte interface, $w = 1$
$\tilde{N} = 0$	$\tilde{N} = \tilde{c}_T \tilde{D} x(1-x) \frac{\partial \tilde{U}}{\partial x} \frac{1}{\tilde{L}} \frac{\partial x}{\partial w} + x(\tilde{N} + \tilde{N}_H)$	$\tilde{N} = \tilde{c}_T \tilde{D} x(1-x) \frac{\partial \tilde{U}}{\partial x} \frac{1}{\tilde{L}} \frac{\partial x}{\partial w} + x(\tilde{N} + \tilde{N}_H)$
$(\partial x/\partial w) = 0$	$\left(x \frac{d\tilde{c}_T}{dx} + \tilde{c}_T\right)\left(\frac{\partial x}{\partial \tau} - \frac{w}{\tilde{L}} \frac{d\tilde{L}}{d\tau} \frac{\partial x}{\partial w}\right) = -\frac{1}{\tilde{L}} \frac{\partial N}{\partial w}$	$(1-x)\tilde{N} - x\tilde{N}_H =$ $\begin{cases} \tilde{i} & \text{current control} \\ \alpha x^{\beta}(1-x)^{1-\beta}\left[e^{(1-\beta)(\tilde{V}-\tilde{U})} - e^{-\beta(\tilde{V}-\tilde{U})}\right] & \text{potential control} \end{cases}$
$\tilde{N}_H = 0$	$\frac{d\tilde{c}_T}{dx}\left(\frac{\partial x}{\partial \tau} - \frac{w}{\tilde{L}} \frac{d\tilde{L}}{d\tau} \frac{\partial x}{\partial w}\right) = -\frac{1}{\tilde{L}} \frac{\partial (\tilde{N} + \tilde{N}_H)}{\partial w}$	$\frac{d\tilde{c}_T}{dx}\left(\frac{\partial x}{\partial \tau} - \frac{w}{\tilde{L}} \frac{d\tilde{L}}{d\tau} \frac{\partial x}{\partial w}\right) = -\frac{1}{\tilde{L}} \frac{\partial (\tilde{N} + \tilde{N}_H)}{\partial w}$ $\tilde{c}_T \frac{d\tilde{L}}{d\tau} = \tilde{N} + \tilde{N}_H$

[a]The four rows of equations can be used to solve for the unknowns x,$\tilde{N}$, $\tilde{N}_H$, and $\tilde{L}$. A listing of the dimensionless groups is provided in eq 22.

deposition gas was maintained at a flow rate of 15 standard cubic centimeters per minute. The deposition was conducted without substrate heating in order to obtain amorphous Si. The film thickness was monitored by a quartz-crystal microbalance. The Si film was transferred directly to another glovebox (Vacuum Atmospheres Nexus) without exposure to air. CR2032 coin cells were assembled with the Si thin film as the working electrode and a lithium foil as the counter-reference electrode. For the potential sweeps, the product νT_{point} (ν being the scan rate and T_{point} being the time per point) was kept constant and equal to 1 mV/point. Thus, in scanning from 1 V to 50 mV, 950 current−voltage data points were collected. A microporous membrane (Celgard, U.S.A.) was used as the separator, and the electrolyte was a mixture of ethylene carbonate and diethyl carbonate (1:1 volume ratio, Novolyte, U.S.A.) with 1 M $LiPF_6$. The linear-sweep voltammetry was carried out with a VMP3 multichannel potentiostat (Bio-Logic).

RESULTS AND DISCUSSION

Dynamic Equilibrium. The low-rate behavior of the Li−Si system is displayed in Figure 2, which we take to be representative of equilibrium. The hysteresis is immediately apparent. We obtain effectively the same open-circuit voltage versus lithium concentration plot at C/40 (40 h per charge or discharge) or 0.01 mV/s (28 h to go from 1 V to 50 mV vs Li). The Supporting Information provides a short derivation of the open-circuit voltage versus lithium concentration for the case of dynamic equilibrium:

$$i = L_0 c_{T,0} F \nu \frac{\partial x}{\partial U} \tag{24}$$

wherein ν is the sweep rate of the potential. In this work, both U and $(\partial x/\partial U)$ are cast as look-up tables (tables of U and $(\partial x/\partial U)$ as functions of x). To use eq 24 to generate a dynamic-equilibrium $i-V$ curve, one sets $U = V$; once V is specified, the look-up table for the $U-x$ relation can be used to identify both x and $(\partial x/\partial U)$, with the latter quantity being used to calculate i per eq 24. The differential voltage spectroscopy plot to the left in Figure 2 shows charge reactions at 0.23 and 0.085 V versus Li, while discharge peaks appear at 0.48 and 0.28 V vs Li. While the differential voltage spectroscopy plot makes the reaction peaks clear, the plots of the open-circuit potential versus state of charge are less indicative. Thus, the differential voltage spectroscopy plot implies that a thermodynamic description of the Li−Si system might be effectively approached by assuming two immiscible components,[4,34,46] perhaps two amorphous phases, within the electrode. In this work, however, we take the pragmatic approach, as mentioned

DOI: 10.1021/jp512585z
J. Phys. Chem. C 2015, 119, 5341−5349

previously, of using a look-up table for the open-circuit potential $U(x)$. The total Coulombic capacity of the electrode at these low rates of operation is 0.227 C or 0.0629 mAh. For the 1 cm diameter electrode, the 1C rate of operation corresponds to 55.6 μA/cm^2. For all of the data shown in the work, the current efficiencies after the fifth cycle were unity to within experimental measurement capability.

Constant-Current Discharge. It is helpful to examine a constant-current discharge for the purposes of understanding the behavior of the equation system as well as how the Li−Si system behaves. We employ parameters extracted from the linear sweep voltammetry experiment discussed below. Results are shown in Figure 4. To set up the simulation, we employed

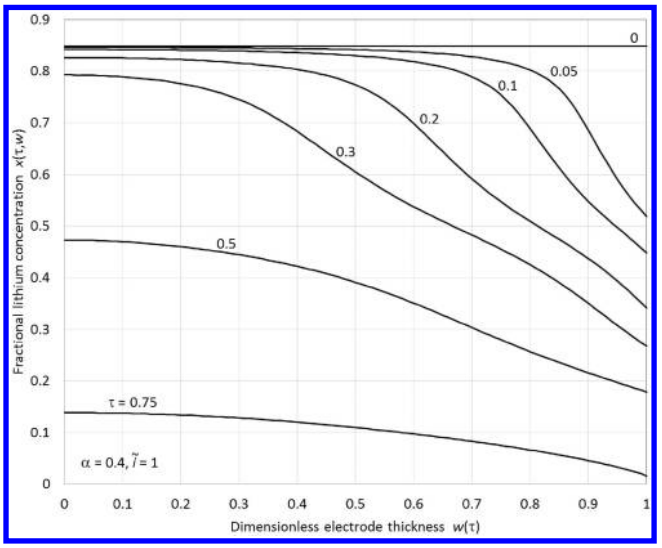

Figure 4. Concentration profiles of lithium filled sites x vs position w throughout a constant current discharge from an initial state of x = 0.848 ($Li_{4.4x}Si$ or $Li_{3.73}Si$ for x = 0.848). Values for $\alpha = L_0 i_0^{ref}/(D_0 c_{T,0} F)$ and $\tilde{i} = iL_0/(D_0 c_{T,0} F)$ are shown. In addition, $\tilde{D} = D/D_0 = 1$.

the definition of the dimensionless current (eq 22), set the current density to 1 mA/cm^2, a value that is desirable for traction applications, and then determined what film thickness L_0 would yield $\tilde{i}$ = 1; for the Li−Si parameters we employed, L_0 = 1.76 μm, a realistic value in terms of particle sizes used in lithium-ion batteries. For the conditions chosen, $\alpha = (L_0/D_0 c_{T,0})(i_0^{ref}/F)$ = 0.4, implying a balance between diffusion and charge-transfer resistance (i.e., both are important in determining the voltage response). Based on capacity measurements for the 67 nm thick electrode, we take the charged state to be x = 0.848 (for $Li_{4.4x}Si$, x = 0.848 corresponds to $Li_{3.73}Si$). Hence, the C-rate for the 1.76 μm film over the concentration range of $0 < x < 0.848$ corresponds to 1.46 mA/cm^2. Thus, the results depicted Figure 4 correspond to about a (2/3)C discharge rate, a value that is of interest with respect to EREV and BEV applications.

The general trend in the concentration profiles depicted in Figure 4 are consistent with treatments of diffusion as depicted, for example, in ref 47. The concentration is initially uniform at x = 0.848. As Li is extracted from the electrode, the concentration at the surface depletes relative to that at the interface with the current collector. Eventually, the Li concentration at the surface falls to near-zero values, and the commanded current can no longer be supplied (at times greater than approximately τ = 0.75).

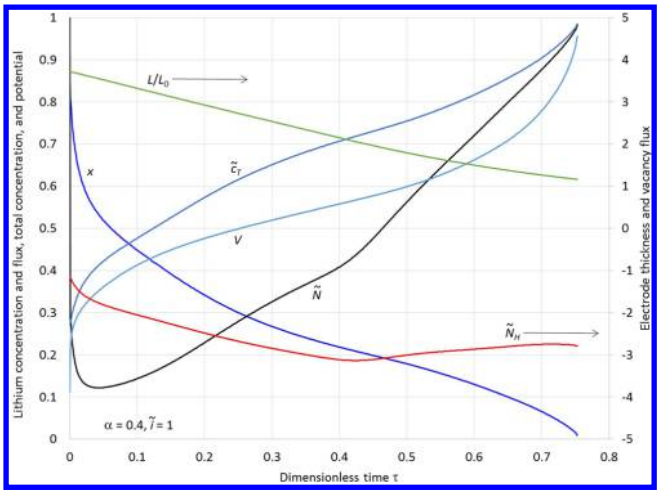

Figure 5. Histories of variables during constant current discharge. The compositions x and $\tilde{c}_T = c_T/c_{T,0}$ as well as the fluxes $\tilde{N} = NL_0/(D_0 c_{T,0})$ $\tilde{N} = NL_0/(D_0 c_{T,0})$ and $\tilde{N}_H = N_H L_0/(D_0 c_{T,0})$ are evaluated at the electrode−electrolyte interface w = 1 ($z = L$). Conditions correspond to values provided in the caption of Figure 4 and β = 0.5. The left ordinate is to be used for curves without an adjacent arrow pointing to the right ordinate.

The variation in key calculated quantities at the electrode−electrolyte interface (w = 1, $z = L$) are displayed in Figure 5. It may be helpful to recall that we treat Li filled sites x and unfilled sites $1 - x$, and that the flux $\tilde{N}_H = N_H L_0/(D_0 c_{T,0})$ should not be confused with a Si flux. As noted previously, equi-molar counter diffusion corresponds to a constant concentration of total sites c_T. Because of the change in c_T with x (cf. Figures 3 and 5), the departure from $\tilde{N} = -\tilde{N}_H$ is significant. The electrode contracts geometrically by $(L_{init} - L_0)/L_0 >$ 250%. The remaining variables, $x(\tau,1)$ and $V(\tau)$, follow trends one would expect, with nonideal variables impacting their histories: the filled-site concentration x declines throughout discharge, and the electrode potential V, relative to a Li reference, rises away from that of the Li electrode as Li is extracted.

Linear-Sweep Voltammetry. We employ a form of linear-sweep voltammetry with potential holds at the start and finish of each scan because of the complex hysteresis seen in the open-circuit potential (cf. Figure 2). By holding the potential at the start and end of each potential scan, we can isolate the charge and discharge phenomena; that is, we can use the discharge OCV curve to treat discharge data, and the charge OCV to treat charge data. The data in Figure 6 for the fastest scan rate (0.5 mV/s) show that for cycles beyond the fourth cycle, the system appears to have obtained a uniform and sustained periodic state (the stationary state). We find these thin-film results to be quite reproducible, although we do not expect such stability for greater than about 20 cycles due to slow deterioration of the electrode.[24] As mentioned previously, from a traction applications perspective, the 1C rate is of interest; i.e., drivers of vehicles are interested in how far they can drive on a time scale of an hour. The current densities of Figure 6 are significantly greater than the 1C rate for the 67 nm-thick film (55.6 μA/cm^2), and we do not examine higher currents than those shown.

The influence of sweep rate on current density is portrayed in Figure 7. Note that the magnitude of the current density tends to zero at the maximum and minimum potentials, as the potential is held constant at the extremes. The dashed curves

DOI: 10.1021/jp512585z
J. Phys. Chem. C 2015, 119, 5341−5349

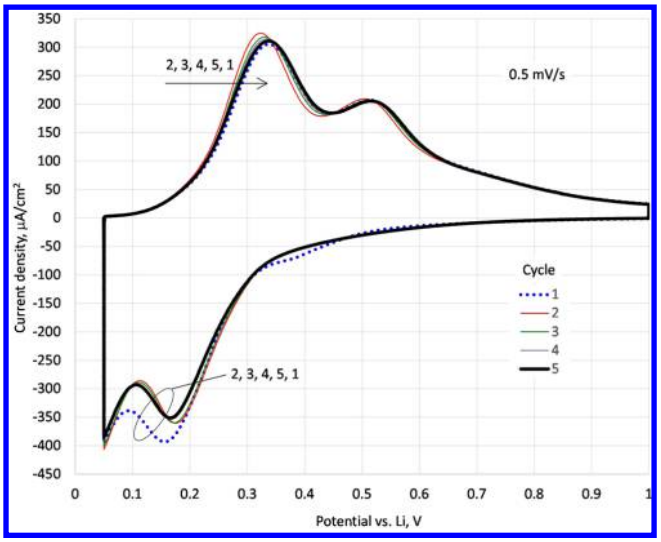

Figure 6. Experimental results for linear-sweep voltammetry from 0 to 0.05 V vs Li. The curves are thicker for cycles 1 and 5. The charge current is highest for the first cycle (particularly between 0.1 and 0.15 V), and a small shoulder in the charge curve is seen near a 0.4 V that does not appear on subsequent cycles.

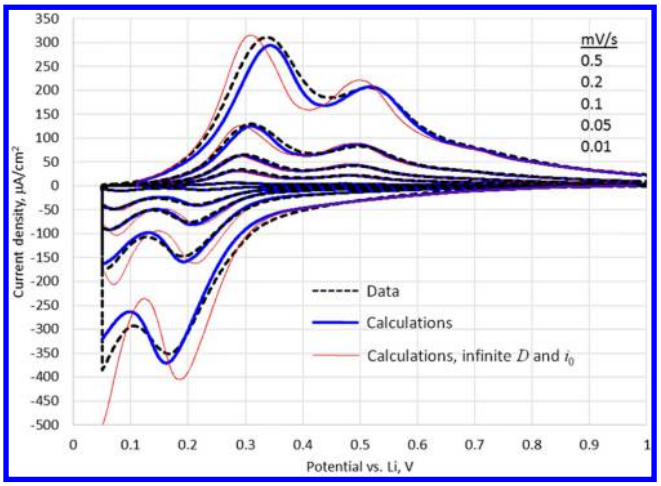

Figure 7. Frequency dependence of the current density during linear-sweep voltammetry. The dashed curves corresponds to data. The thick lines display the calculations (Table 3 for the equation system used to generate the calculations and Table 4 for parameters and properties). The thin lines corresponds to infinite values for D_0 and i_0^{ref} (cf. eq 24) and may be viewed as the dynamic equilibrium response.

corresponds to data, and the thick lines display the calculations resulting from the equation system presented in Table 3 with $D_0 = 5 \times 10^{-12}$ cm^2/s and $i_0^{ref} = 0.4$ mA/cm^2 (cf. Table 4 for all values used to generate the model curves). The thin lines correspond to infinite values for D_0 and i_0^{ref} (cf. eq 24) and may be viewed as the dynamic equilibrium response. For scan rates below about 0.05 mV/s, the system appears to be in dynamic equilibrium as plotted; it is interesting that the maximum charge current density at 0.05 mV/s is near the 1C value (55.6 μA/cm^2), implying that nearly reversible operation is achieved for currents at our below the 1C rate for the thin film electrode. Relative to the (dynamic) equilibrium current−potential results, adding diffusion and interfacial resistance (i) shifts the $i-V$ curves to lower potentials on charge (lithiation of the film) and higher potentials on discharge, and (ii) reduces the magnitude of the current density. To summarize the results of Figure 7, the $i-V$ curves at very slow scan rates take on a form similar to the differential voltage spectroscopy plots ($(\partial x/\partial U)$ versus U, left plot of Figure 2). In this work, the highest scan rate is 0.5 mV/s or 0.0005 V/s, and the fit values of L_0^2/D_0 correspond to about 9 s, far less than the duration required to sweep the potential between maximum and minimum values for the experiments depicted in Figure 7. For the highest scan rate of 0.5 mV/s, 1900 s are required to scan between 1 and 0.05 V. Note that both x and U (with units of Volts) vary from 0 to 1 in this work; thus $(\partial x/\partial U)$ is of order one, $\nu L_0^2/D_0 < 0.005$ V, $\tilde{i}$ is small even at the highest scan rate, and the dynamic equilibrium analysis is a helpful benchmark calculation, consistent with the thinnest curves in Figure 7 providing an approximate representation of the data depicted in Figure 7.

Table 4. Parameters and Properties for Calculations[a]

parameter or property	value	units	explanation
D_0	5×10^{-12}	cm^2/s	fit to data
L_0	67×10^{-7}	cm	measured
$i_{0,ref}$	0.4×10^{-3}	A/cm^2	fit to data
β	0.5		refs 32 and 55
$\frac{L_0^2}{D_0}$	9	s	calculated based on fit values
$\alpha = \frac{L_0}{D_0 c_{T,0}} \frac{i_0^{ref}}{F}$	0.0152		calculated based on fit values

[a]For this work, it was assumed that $\tilde{D} = D/D_0 = 1$.

The plots in Figure 8 help one to assess the departure from equilibrium associated with the curves in Figure 7. Plotted are the lithium concentration, x in $Li_{4.4x}Si$, at the current collector surface $w = z = 0$ (lower four curves) and the variation in film thickness L/L_0, or fractional volume change, (upper four curves) for the slowest scan rate (0.01 mV/s) and highest scan rate (0.5 mV/s). As plotted, the 0.01 mV/s data cannot be resolved from those for the dynamic equilibrium case. On charge at low rates (e.g., 0.01 mV/s and lower), the film volume expands by 270%, consistent with the discussion of eq 8. At 0.5 mV/s, the expansion is just over 200%; the higher scan rate reduces that amount of lithium that can be placed in the film during the experiment, consistent with the plots of $x(t,0)$ in Figure 8, leading to less expansion. For the charge experiments, the system is initially equilibrated at 1 V versus Li, and very little Li is in the film. As the potential is scanned linearly to its lowermost value, the current rises, and the influence of irreversible phenomena increases. In contrast, for the discharge experiments, the system is equilibrated initially, and it is near an equilibrium state as the potential approaches 1 V versus Li. Hence, the charge curves show a greater disparity relative to those of dynamic equilibrium as compared to the discharge curves.

Thin-film electrodes can be used to reduce diffusion resistance relative to that of charge transfer. This fact is the basis for the use of microelectrodes to probe interfacial phenomena without the intrusion of diffusion resistance. In the treatment of microdisk electrodes, as in this work, the symbol α has been used to represent a dimensionless group that includes the characteristic electrode size and reflects the ratio of diffusion resistance to that of charge transfer.[46−51] An electrochemical Biot number B has also been employed for this purpose in the context of spherical particles.[52−54] In the field of heat transfer, the Biot number provides a measure of the ratio of the heat-transfer resistance inside a solid relative to that at its surface.[39]

DOI: 10.1021/jp512585z
J. Phys. Chem. C 2015, 119, 5341−5349

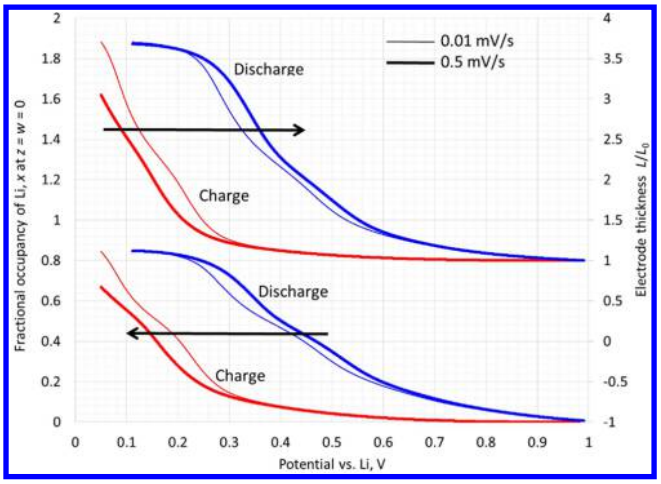

Figure 8. Lithium concentration, x in $Li_{4.4x}Si$, at the current collector surface $x(t,0)$ (lower four curves) and variation in film thickness L/L_0, or fractional volume change, (upper four curves) for the slowest scan rate (0.01 mV/s) and highest scan rate (0.5 mV/s). The 0.01 mV/s data, as plotted, cannot be resolved from those for the dynamic equilibrium case (cf. eq 24).

For the 67 nm thick film used in this work, $\alpha = (L_0/D_0c_{T,0})\, i_0^{ref}/F = 0.0152$, implying far less diffusion resistance than that associated with charge transfer. As a result, we find that the sensitivity to diffusion coefficient values greater than $D_0 = 5 \times 10^{-12}$ cm^2/s is not significant. Thus, we conclude from the results depicted in Figure 9 that the Li diffusion coefficient

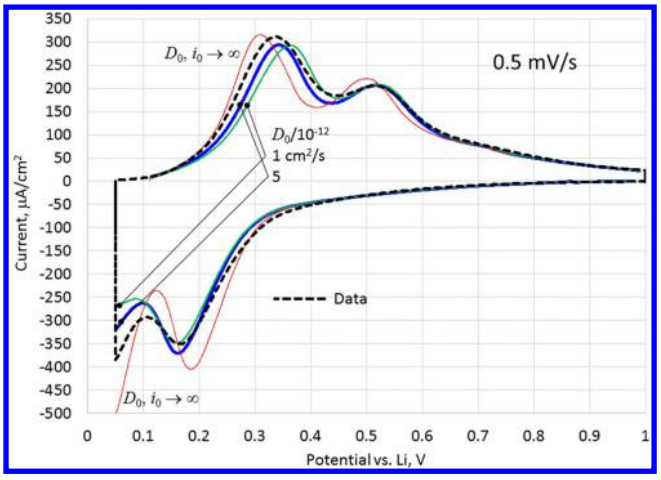

Figure 9. Sensitivity to the value of the Li diffusion coefficient. For values greater than $D_0 = 5 \times 10^{-12}$ cm^2/s, little sensitivity is observed. The dynamic equilibrium case (cf. eq 24) corresponds to the curve labeled D_0, $i_0 \to \infty$.

must be at least 5×10^{-12} cm^2/s to provide a good fit of the data, but we cannot resolve the impact of higher values. In contrast, good sensitivity is obtained relative to the exchange current density, as is indicated in Figure 10. We find a value of $i_0^{ref} = 0.4$ mA/cm^2 provides the best representation of the data for the values investigated above and below the fit value.

SUMMARY AND OPEN QUESTIONS

We have derived an equation system for the treatment of electrode materials that undergo large volume changes during operation; the dimensioned formulation is provided in Table 2,

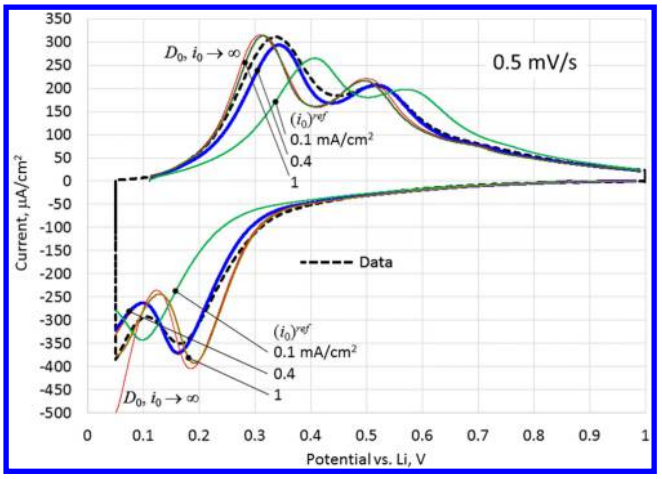

Figure 10. Sensitivity to the value of the exchange current density. Consistent with the small value of $\alpha = L_0 i_0^{ref}/D_0 c_{T,0} F = 0.0152$, kinetic resistance at the electrode−electrolyte interface is much greater than that of diffusion for the thin-film electrode, and the results are quite sensitive to the value of the exchange current density. The dynamic equilibrium case (cf. eq 24) corresponds to the curve labeled D_0, $i_0 \to \infty$.

and Table 3 depicts the dimensionless formulation. The approach is applied to a thin-film Li−Si system, wherein a volume change of about 270% is observed relative to pure Si and $Li_{3.75}Si$. Good agreement is obtained when the model calculations are compared with experimental data obtained from Li−Si thin film electrodes (67 nm thickness) subjected to linear-sweep voltammetry experiments over current and potential ranges of interest for many applications, including electrified vehicles (cf. Figure 7).

Significant open questions must be addressed in future work. First, the system thermodynamics has been rendered as a look-up table. It is likely that the Li−Si thin film is amorphous upon cycling, and the differential voltage spectroscopy results (left plot of Figure 2) are thus consistent with two reactions. It may be that a treatment involving two immiscible, amorphous phases is needed. Complicating matters further, at very low rates of current passage (i) the hysteresis is large (right plot of Figure 2) and (ii) the peak potentials upon charge and discharge are quite different (left plot of Figure 2). It is clear that understanding the thermodynamics of such Li−Si systems is challenging. Upon resolution of the system thermodynamics, it would then be appropriate to revisit the speciation of the solid state and re-evaluate diffusion coefficients and exchange current densities. We note that calculations presented for 0.5 mV/s scan-rate yield currents greater in magnitude than the first measured current peak (near 0.18 V vs Li) and currents lower in magnitude than those measured near the end of the charge scan. We could obtain a better fit by allowing, for example, the exchange current density and the dimensionless diffusion coefficient $\tilde{D} = D/D_0$ (set to unity in this work) to vary with lithium concentration, but the value of such an endeavor is questionable given the approximate treatment of the system thermodynamics and speciation. Last, as discussed, we neglect the influence of stress on lithium diffusion, consistent with an infinitely thin film or a vanishing small elastic modulus or both; while this simplifies the analysis, it is beyond the scope of this work to assess the error associated with this approximation.

DOI: 10.1021/jp512585z
J. Phys. Chem. C 2015, 119, 5341−5349

■ ASSOCIATED CONTENT

Supporting Information

Additional theoretical details. This material is available free of charge via the Internet at http://pubs.acs.org.

■ AUTHOR INFORMATION

Notes

The authors declare no competing financial interest.

■ ACKNOWLEDGMENTS

The authors thank Dr. Daad Haddad for the EPMA (electron microprobe analysis) for the thickness measurements of the silicon films. Q.L.Z. and Y.T.C. acknowledge partial support from National Science Foundation Award No.1355438 (Powering the Kentucky Bioeconomy for a Sustainable Future).

■ REFERENCES

(1) Harris, W. S. Electrochemical Studies in Cyclic Esters. *Ph.D. Thesis*; University of California: Berkeley, CA, 1958.
(2) Xu, K. *Chem. Rev.* **2004**, *104*, 4303.
(3) Whittingham, M. S.; Jacobson, A. J. *Intercalation Chemistry*; Academic Press: New York, 1982.
(4) Winter, M.; Besenhard, J. O.; Spahr, M. E.; Novák, P. *Adv. Mater.* **1998**, *10*, 725−763.
(5) Whittingham, M. S. *Chem. Rev.* **2004**, *104*, 4271−4301.
(6) Lacher, D.; Beattie, S.; Morcrette, M.; Edström, K.; Jumas, J.-C.; Tarascon, J.-M. *J. Mater. Chem.* **2007**, *17*, 3759−3772.
(7) Yoshio, M.; Brodd, R. J.; Kozawa, A. *Lithium-Ion Batteries*; Springer: New York, NY, 2008.
(8) Huggins, R. A. *Advanced Batteries: Materials Science Aspects*; Springer: New York, NY, 2009.
(9) Nazri, G. A.; Pistoria, G. *Lithium Batteries: Science and Technology*; Springer: New York, NY, 2009.
(10) Goodenough, J. B.; Kim, Y. *J. Power Sources* **2011**, *196*, 6688.
(11) Timmons, A. T. Visible Changes in Lithium-Ion Electrodes Upon Lithium Insertion and Removal. *Ph.D. Thesis*; Dalhousie University: Halifax, Nova Scotia, 2007.
(12) Obrovac, M. N.; Christensen, L.; Le, D. B.; Dahn, J. R. *J. Electrochem. Soc.* **2007**, *154*, A849.
(13) Zeng, Z.; Liu, N.; Zeng, Q.; Ding, Y.; Qu, S.; Cui, Y.; Mao, W. L. *J. Power Sources* **2013**, *242*, 732.
(14) Thomas, K. E.; Darling, R.M.; Newman, J. Mathematical Modeling of Lithium Batteries. In *Advances in Lithium-Ion Batteries*; van Schalkwaijk, W., Scrosati, B., Eds.; Kluwer: Dordrecht, 2002; Chapter 12.
(15) Newman, J.; Thomas-Aleya, K. E. *Electrochemical Systems*, 3rd ed.; Wiley: New York, NY, 2004.
(16) Baker, D. R.; Verbrugge, M. W. *J. Electrochem. Soc.* **2013**, *160*, A1.
(17) Baker, D. R.; Li, C.; Verbrugge, M. W. *J. Electrochem. Soc.* **2013**, *160*, 1794.
(18) Chandrasekaran, R.; Magasinski, A.; Yushin, G.; Fuller, T. F. *J. Electrochem. Soc.* **2010**, *157*, A1139.
(19) Graetz, J.; Ahn, C. C.; Yazami, R.; Fultz, B. *Electrochem. Solid-State Lett.* **2003**, *6*, A194.
(20) Ohara, S.; Suzuki, J.; Sekine, K.; Takamura, T. *J. Power Sources* **2004**, *136*, 303.
(21) Uehara, M.; Suzuki, J.; Tamura, K.; Sekine, K.; Takamura, T. *J. Power Sources* **2005**, *146*, 441.
(22) Takamura, T.; Uehara, M.; Suzuki, J.; Sekine, K.; Tamura, K. *J. Power Sources* **2006**, *158*, 1401.
(23) Soni, S. K.; Sheldon, B. W.; Xiao, X.; Tokranov, A. *Scr. Mater.* **2011**, *64*, 307.
(24) Xiao, X.; Liu, P.; Verbrugge, M. W.; Haftbaradaran, H.; Gao, H. *J. Power Sources* **2011**, *196*, 1409.
(25) Li, J.; Yang, F.; Cheng, Y.-T.; Verbrugge, M. W.; Xiao, X. *J. Phys. Chem. C* **2012**, *116*, 1472.
(26) Soni, S. K.; Sheldon, B. W.; Xiao, X.; Verbrugge, M. W.; Ahn, D.; Haftbaradaran, H.; Gao, H. *J. Electrochem. Soc.* **2012**, *159*, A38−A43.
(27) Martin, L.; Martinez, H.; Ulldemolins, M.; Pecquenard, B.; Le Cras, F. *Solid State Ionics* **2012**, *215*, 36.
(28) Haftbaradaran, H.; Xiao, X.; Verbrugge, M. W.; Gao, H. *J. Power Sources* **2012**, *206*, 357.
(29) Soni, S. K.; Sheldon, B. W.; Xiao, X.; Bower, A.; Verbrugge, M. W. *J. Electrochem. Soc.* **2012**, *159*, A1520.
(30) Li, J.; Xiao, X.; Cheng, Y.-T.; Verbrugge, M. *J. Phys. Chem. Lett.* **2013**, *4*, 3387.
(31) Zhang, Q.; Xiao, X.; Cheng, Y.-T.; Verbrugge, M. W. *Appl. Phys. Lett.* **2014**, *105*, 061901.
(32) Verbrugge, M. W.; Koch, B. J. *J. Electrochem. Soc.* **1996**, *143*, 600.
(33) Verbrugge, M. W.; Koch, B. J. *J. Electrochem. Soc.* **1999**, *146*, 833.
(34) Baker, D. R.; Verbrugge, M. W. *J. Electrochem. Soc.* **2012**, *159*, A1341.
(35) Sethuraman, V. A.; Srinivasan, V.; Bower, A. F.; Guduru, P. R. *J. Electrochem. Soc.* **2010**, *157*, A1253.
(36) Bower, A. F.; Guduru, P. R.; Sethuraman, V. A. *J. Mech. Phys. Solids* **2011**, *59*, 804.
(37) Sheldon, B. W.; Soni, S. K.; Xiao, X.; Qi, Y. *Electrochem. Solid-State Lett.* **2012**, *15*, A9.
(38) Bucci, G.; Nadimpalli, S. P.V.; Sethuraman, V. A.; Bower, A. F.; Guduru, P. R. *J. Mech. Phys. Solids* **2014**, *62*, 276.
(39) Bird, R. B.; Stewart, W. E.; Lightfoot, E. N. *Transport Phenomena*; Wiley: New York, 1960.
(40) Obrovac, M. N.; Christensen, Leif *Electrochem. Solid-State Lett.* **2004**, *7*, A93.
(41) Li, J. *Metall. Trans. A* **1978**, *9A*, 1353.
(42) Boukamp, B. A.; Lesh, G. C.; Huggins, R. A. *J. Electrochem. Soc.* **1981**, *128*, 725.
(43) Darken, L. S. *Technical Publication No. 2311, Class E, Metals Technology*; American Institute of Mining and Metallurgical Engineers: Englewood, CO, 1948; pp 1−11.
(44) Christensen, J.; Newman, J. *J. Solid State Electrochem.* **2006**, *10*, 293.
(45) Verbrugge, M. W.; Gu, H. Finite Difference Routines for One and Two Dimensional Problems Utilizing a Functional Programming Style, PV 94−22. In *Topics in Electrochemical Engineering*; Newman, J., White, R. E., Eds.; Proceedings of the Douglas N. Bennion Memorial Symposium; The Electrochemical Society: Pennington, NJ, 1994.
(46) Verbrugge, M. W.; Koch, B. J. *J. Electrochem. Soc.* **2003**, *150*, A374.
(47) Crank, J. *The Mathematics of Diffusion*; Oxford University Press: London, 1956; pp 58−59.
(48) Baker, D. R.; Verbrugge, M. W. *J. Electrochem. Soc.* **1990**, *37*, 1832.
(49) Baker, D. R.; Verbrugge, M. W. *J. Electrochem. Soc.* **1990**, *137*, 3836.
(50) Verbrugge, M. W.; Baker, D. R. *J. Phys. Chem.* **1992**, *96*, 4572.
(51) Verbrugge, M. W.; Baker, D. R. *J. Electrochem. Soc.* **1996**, *143*, 2252.
(52) Cheng, Y.-T.; Verbrugge, M. W. *J. Electrochem. Soc.* **2010**, *157*, A508.
(53) Cheng, Y.-T.; Verbrugge, M. W. *Electrochem. Solid-State Lett.* **2010**, *13*, A128.
(54) Li, J.; Yang, F.; Cheng, Y.-T.; Xiao, X.; Verbrugge, M. W. *Electrochim. Acta* **2012**, *75*, 56.
(55) Verbrugge, M. W.; Koch, B. J. *J. Electrochem. Soc.* **1994**, *141*, 3053.

DOI: 10.1021/jp512585z
J. Phys. Chem. C 2015, 119, 5341−5349